Deciphering Structural and Ferroelectric behaviour in $Hf_{1-x}Zr_xO_2$ Thin Films through Chemical Beam Vapor Deposition

Md Kashif Shamim [1], William Maudez [2], Estelle Wagner [2], Digvijay Narayan Singh[3], Seema Sharma[1], Giacomo Benvenuti [2, 4] and Rashmi Rani[2, *]

[1]Material Research Laboratory, Department of Physics, A N College, Patna-800013, India

[2]3D-OXIDES, 41 Rue Henri FABRE, SAINT GENIS POUILLY, 01630, France

[3]Department of Materials Engineering, Indian Institute of Science, Bengaluru-560012, India

[4]ABCD Technology, Route de Champ-Colin 12, CH-1260, Nyon, Switzerland

* Corresponding Author: Rashmi Rani   Email**:** rashmi.rani@3d-oxides.com (Rashmi Rani)

Abstract

The discovery of ferroelectricity (FE) in hafnium-based thin film system has opened a new avenue of research, where HfO_2 is considered a suitable replacement for Si-based electronic devices. However, the occurence of FE and its underlying physical mechanism is not well understood. In this paper, we report the synergistic role of defect dipoles on the structure, electrical, and ferroelectric behavior of $Hf_{0.7}Zr_{0.3}O_2$ (Hf-rich), $Hf_{0.5}Zr_{0.5}O_2$ (50-50), $Hf_{0.3}Zr_{0.7}O_2$ (Zr-rich) thin films grown on TiO_2: Nb substrate using Chemical Beam Vapor deposition (CBVD) technique. Grazing angle incidence X-ray diffraction (GIXRD) and Raman measurements confirm the coexistence of the monoclinic and orthorhombic phases in the films. Detailed X-ray Photoelectron Spectroscopy (XPS) analysis showed the coexistence of metallic and oxide cationic forms of Hf, which ratify the presence of defect dipoles. These defect dipoles significantly affect the electrical and ferroelectric behavior of the films. A lossy

polarization behavior was observed for 50/50 and Zr-rich films. The negative shift of polarization loops a supports the antistites disordering in the systems. A maximum dielectric constant of ~16 and a minimum value of ~7 was recorded for Hf-rich and Zr-rich films at 100Hz frequency.

Keywords: $Hf_{1-x}Zr_xO_2$; Thin Film; Chemical Beam Vapor deposition; Ferroelectricity; Defect Dipoles.

Introduction

Hafnium oxide (HfO_2) is a wide band-gap semiconductor (Eg ~4.5 eV) material that exhibits high dielectric constant k~20 value, high chemical, and thermal stability and is considered as a potential successor of Si-based gate dielectric for next generation electronic device applications [1-3]. In 2011, Boscke [4] observed ferroelectric (FE) behavior in Si-doped HfO_2 film, which was attributed to some metastable polar phase formation referred to as the polar orthorhombic phase with the space group $Pca2_1$. In HfO_2, different polymorphs exist, i.e., monoclinic phase with $P2_1/C$ space group, which transforms to a tetragonal phase at 1700^0C and further to a cubic phase at 2600^0C [5, 6]. These polymorphs are centrosymmetric; hence non-ferroelectric behavior could be observed for all of them [6, 7]. Additionally, at room temperature, the most stable monoclinic phase also lacks the necessary non-centrosymmetric condition, which is required to develop spontaneous polarization in Hf-based systems.

So, it was proposed that doping and confinement of HfO_2 film may lead to a stage where the system undergoes a phase transition from centrosymmetric to polar non-centrosymmetric phase and exhibits FE behavior. Ever since then, ferroelectricity (FE) has been reported by Sang et al. [8] in Gd-doped and undoped HfO_2 thin films. Pressure-induced FE phase was also observed in Si-doped HfO_2 film [4]. Recent reports are piled up with examples of FE films with a series of dopants such as Al [9], La [10], Zr [11], Si [4], Gd [12], Sr [13], and Y [14] deposited on different substrates TiN [15], Pt [16], and TaN [12] via different deposition techniques; Atomic Layer Deposition ALD [15], Pulsed Laser Deposition PLD [17], Chemical vapor deposition CVD [18], Chemical Solution deposition (CSD) [19], and many more. Apart from the above-mentioned factors, stress, top and bottom electrodes, interlayer diffusions, surface energy, and defect also play a vital role in stabilizing the FE phase in a Hf-

based system [20]. Since then the synthesis film depositional parameters have becomes a decisive factor for achieving metastable orthorhombic phase in Hf system. In the initial phase, FE was observed in films with <10nm thickness, and when the thickness was increased m-phase started dominating, and FE behavior was compromised [3,4, 17]. FE was also observed in 50nm thick hafnium-zirconium film with laminated structure and Al_2O_3 at the interlayers [21]. From the above studies, it was concluded that FE in Hf-based films could originate, provided that the average grain size is small, which aids in stabilizing the metastable orthorhombic (o)- phase. For films with thickness >10nm, m-phase always exists, and the o-phase can be hypothesized as the transformation between the tetragonal and m-phase.

Different film deposition techniques and dopants have been explored to stabilize the metastable orthorhombic phase to achieve FE in HfO_2 thin films. Chemical Beam Vapor Deposition through a combinatorial approach gives the flexibility of depositing high-quality thin films with precise control over the depositional parameters, and our previous report confirms the statement [22]. Among dopants, Zr resembles Hf in structure and chemical stability and can undergo a series of polymorphic formulations. Also, Hf and Zr have comparable ionic radii to contract the lanthanide series; therefore, it is pretty interesting to probe the effect of Zr substitution in the HfO_2 lattice. Hence, Hf and Zr were taken as the precursors, and $Hf_{1-x}Zr_xO_2$ (x=0.0.7,0.5,0.3) were deposited via CBVD to study the structure and correlate electric and ferroelectric properties of the $Hf_{1-x}Zr_xO_2$ thin films (HZO) films.

Materials and Methods

The deposition of combinatorial HZO composite thin film onto the TiO_2:Nb substrate (house made) was carried out using the SYBILLA P200 equipment from ABCD Technology via CBVD method. The complete details of the film deposition and equipment can be found in our previous work [**23**]. Hafnium 2-methoxymethyl-2-propoxide (CAS N° 309915-48-8) (Hf(mmp)$_4$) from Sigma Aldrich and Zirconium-2-methyl-2-butoxide (CAS 24675-20-5) (Zr(OMBu)$_4$) from Gelest were selected as the starting precursors.

The deposition parameters of the HZO composite films are shown in Table 1.

Table 1 Experimental parameters for CBVD growth

Precursor	T precursors (°C)	T substrate (°C)	P chamber (Pa)	Deposition time (minute)	Substrate
Hafnium 2-methoxymethyl-	87±0.1	500	4.9	60	TiO$_2$:Nb

2-propoxide (Hf(mmp)₄)					
Zirconium-2-methyl-2-butoxide (Zr(OMBu)₄)	57±0.1	500	6.6	60	TiO$_2$:Nb

Characterization

X-ray diffraction (XRD; Bruker D8 Advance) equipped with Cu kα radiation (λ = 1.5406 Å) and ώ-2º was employed to study and identify the crystal structure of the grown films. Room temperature Raman spectroscopy measurement was performed using excited radiation of 438 nm (Micro Raman spectrometer from Jobin Yvon Horibra LABRAM-HR), and the spectrum was recorded in the range of 100–1750 cm^{-1}. Au top electrode was sputtered on the prepared films via shadow masking and was heated at 300°C for 30 minute for ferroelectric and electrical characterizations. The chemical states of the cations were ascertained by X-ray photoelectron spectroscopy (XPS) using the Al-Kα (kλ ~ 0.834 nm) lab source. An Omicron energy analyzer (EA-125 Germany) was employed throughout the measurement. Leakage current measurements were performed using the "Radiant Premier Precision II System" (Radiant Technologies, USA) at room temperature and 10 Hz field frequency. Room temperature ferroelectric measurement was carried out at 10Hz using Radiant- II precision , USA. The film's dielectric constant and loss tangent were measured using a Hioki LCR meter in a frequency range of 100 Hz to 1 MHz at room temperature.

Results and Discussions

Structural Analysis

Fig. 1 shows the GIXRD pattern of the HZO thin films recorded at room temperature, keeping ω ~2°. The primary observation suggests the presence monoclinic phase, but the broadening nature of the peak at 2θ ~ 32° and 35° indicates the existence of a secondary phase in the grown films. The observed reflections match well with monoclinic and orthorhombic phase symmetry with space groups; *P21/c* and *Pnma,* respectively. The observed Braggs reflections were indexed based on JCPDS No.: 00-001-750, 00-00600318 for monoclinic ZrO$_2$ and HfO$_2$, and 01-087-2105 and 01-087-0216 for orthorhombic ZrO$_2$ and HfO$_2$ phase symmetry. Although Hf and Zr have comparable ionic radii (85pm and 86pm.), a considerable shift of the peaks towards a higher angle with increasing Zr-ratio indicates a distorted-lattice crystal

symmetry of these system. this is not a common phenomenon feature observed in Hf-Zr-based thin films. Also, it is observed that the evolution of the orthorhombic phase becomes more decisive in the Zr-rich system. The increasing intensity and decreasing broadening of the peak at ~35° confirm this observation. One of the possible reasons for such structural evolution is the complex valence state of the cations existing in the system. Such cationic disordering affects the overall dipole ordering and physical characteristics of the system, and can be attributed to the cationic charge ordering in the films. These results are consistent with the previous reports [24-27].
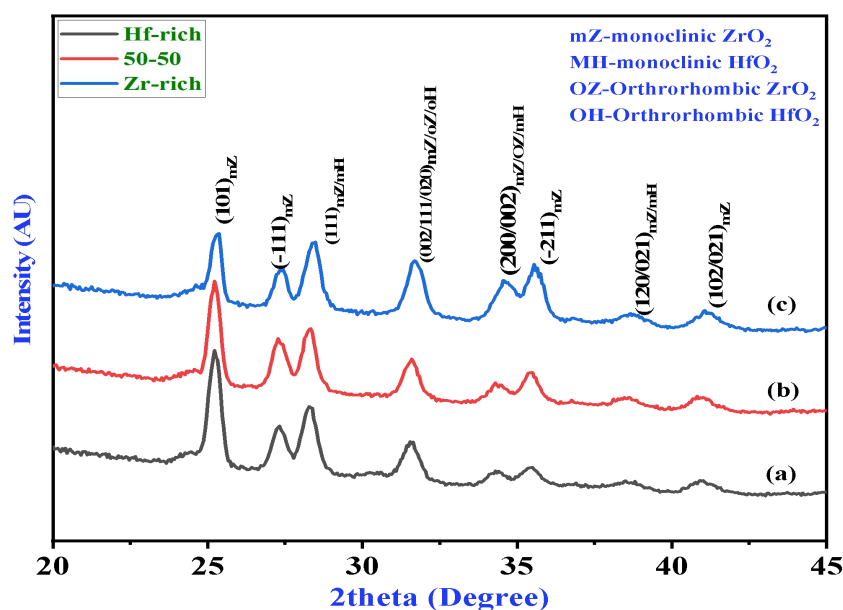
Figure 1: GIXRD of HZO thin films, (a) Hf-rich film, (b) Hf-Hz (50:50) film and (c) Zr-rich film.

Raman analysis

The Lorentzian-fitted Raman spectra of HZO films are represented in Fig-2(a-f). Whole spectra are divided into two regions to get a better view of the active phonon modes present in the films. In Hf and Zr systems, the monoclinic phase is the most stable symmetry observed at room temperature. Theoretically, 18 active ($9A_g+9B_g$) Raman modes for monoclinic and 36 phonon modes ($9A_g+9B_{1g}+9B_{2g}+9B_{3g}$) for orthorhombic are reported [28]. However, the accurate mode assignment is still controversial due to mode broadening and their weaker observed intensities. Here, the observed modes at $147 cm^{-1}$ (B_2g), $158 cm^{-1}$(B_{1g}), $227 cm^{-1}$(B_{1g}), $303 cm^{-1}$(B_{1g}), and $633 cm^{-1}$(A_g), can be assigned to orthorhombic phase with space group Pnma [29], while modes at $373 cm^{-1}$($B_{1g}+A_g$), $436 cm^{-1}$(E_g), $618 cm^{-1}$(A_g+B_{3g}), $644 cm^{-1}$(B_{1u}), and $667 cm^{-1}$(E_g+A_g) assigned to the monoclinic phase of the films. Similar behavior was

observed for 50-50 and Zr-rich films. The above findings infer that the m/o phase coexists simultaneously in the films and is consistent with XRD findings.
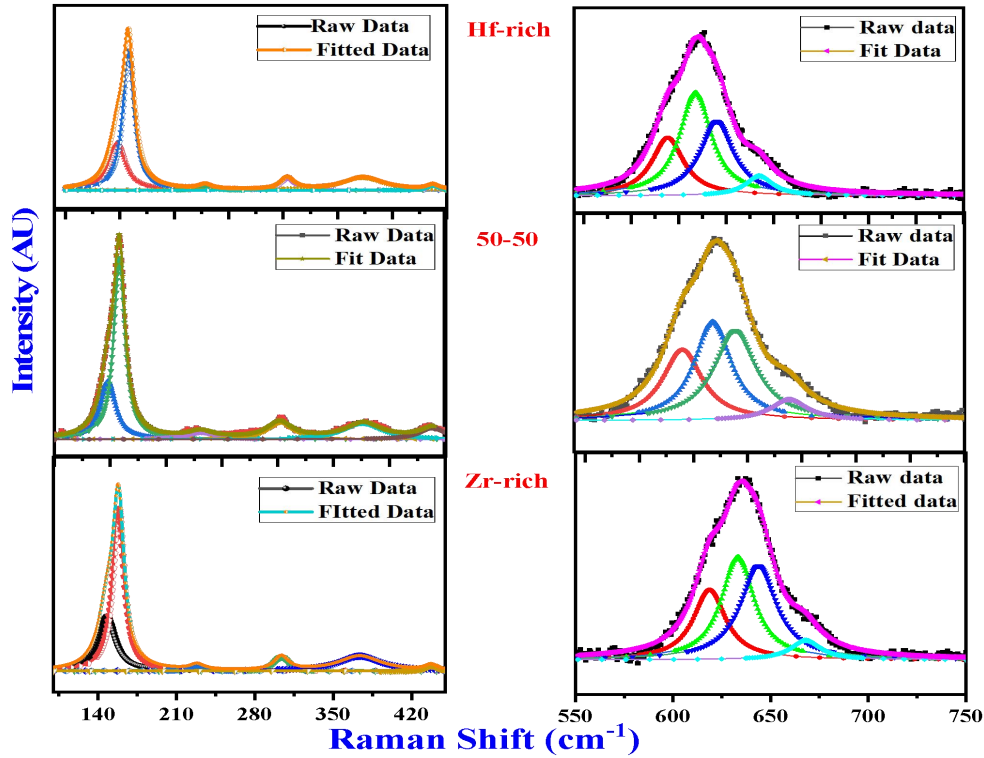
Figure 2: Lorentzian fitted Raman spectra of HZO thin films, two separate spectra of each film are shown to understand the active phonon modes better.

X-ray photoelectron spectroscopy analysis

X-ray photoelectron spectroscopy measurements were carried out at room temperature for O1s, Zr-3d, and Hf-4d cations to probe the oxygen vacancies and its impact on the ferroelectric behavior. Here, the XPS spectra of HZO 50-50 films are analyzed, and other films recorded similar spectra (fig not included here). Initially, the C1s spectrum was recorded, and the binding energy position 284.6 eV was taken as a standard reference for all other cations. A sum of Lorentzian and Gaussian functions was applied to analyze the XPS spectra. Fig-3(a) depicts O1s spectra fitted with two different features (a) Lattice oxygen O_L observed at 530.2eV and the other (b) oxygen vacancies O_D at 531.2 eV ascribed to hydroxy group or HfO. Also, the broad feature of the peaks indicates the gesture of the oxygen vacancy. The deconvoluted spectra of the Zr-3d are shown in the Fig-3(b), which shows two features ascribed to Zr-3$d_{5/2}$ and Zr3$d_{3/2}$ observed at 179.2eV and 181.7eV, confirming that Zr is present in +4 oxidation state.

The deconvoluted spectra of the Hf-4d are shown in fig-3(c). The spectra were fitted with 4 features assigned to a mixed state of Hf and HfO_2. The peaks observed at the binding energy positions 213.6eV and 224.5eV could be assigned to Hf-4$d_{5/2}$ and Hf-4$d_{3/2}$, while the energy positions 215.3eV and 226.3eV can be assigned to HfO_2-4d$_{5/2}$ and HfO_2-4d$_{3/2}$ ions respectively. This confirms that Hf is present in the +4 oxidation state. This can be further correlated with O_{1s} spectra where oxygen vacancies are present.
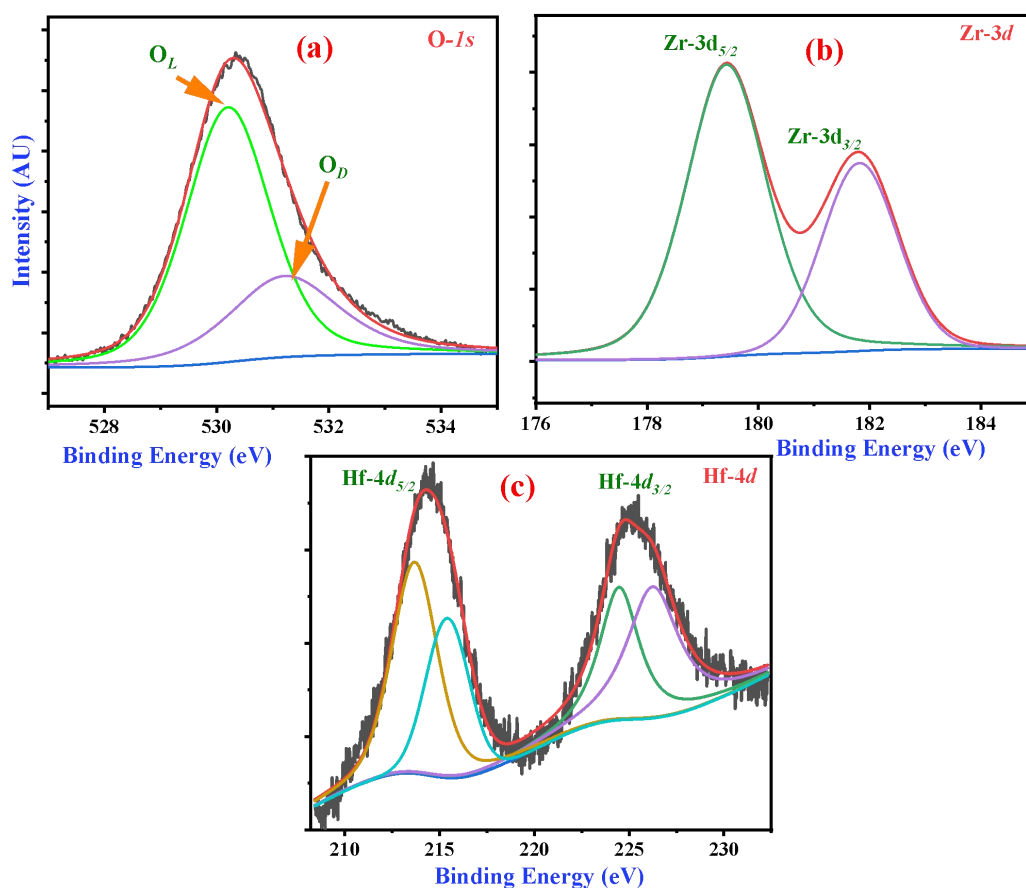
Figure 3: Deconvoluted XPS Spectra (a) O1s (b) Zr-3d core level (c) Hf-4d core level of HZO film

Leakage Current Density analysis

The J-V characteristics of the HZO films, recorded at room temperature, are shown in Fig. 4, where the current density of the Hf-rich film is lower than that of the other two films. As observed in XPS, increasing Zr-content produces a Hf-charge instability that might create defects in the samples. These vacancies procreate mobile charges, increasing the current density of the system. Also, the observed current density of the Zr-rich film is lower than 50-50 film, confirming that Hf cations are the origin of such charge instability.
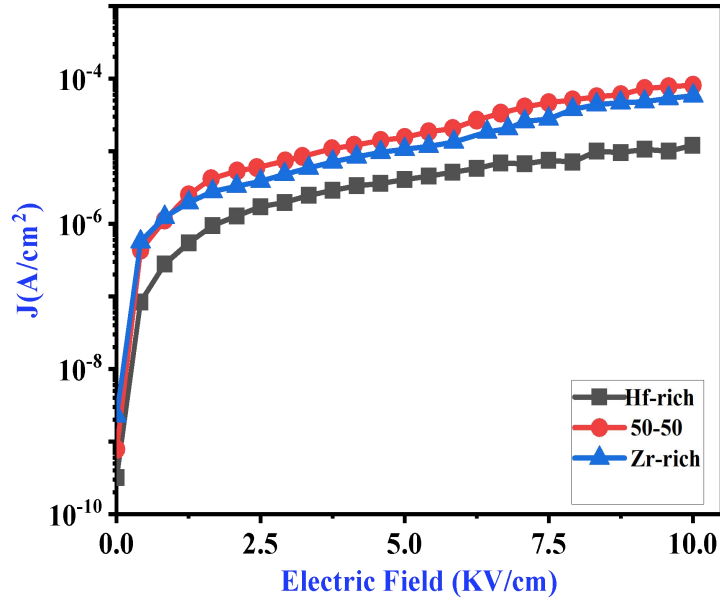
Figure 4: Current density as a function of the applied electric field.

Ferroelectric analysis

Fig. 5 shows the polarization behavior of the HZO films as a function of the applied electric field (EF). All three polarization loops (PE) (Fig. 5 (a-c)) show the lossy ferroelectric characteristics of the studied systems. To explain the effect of defect dipoles on the ferroelectric behavior of HZO films, we focused on the PE loop of 50-50 films (see Fig. 5 (b)). Here, a considerable gap in the start and end point polarization $\sim$ 9 $\mu C/cm^2$, and the system shows a remnant polarization (P_r) of ~12 ($\mu C/cm^2$). Therefore, in a complete cycle of EF, the system contains a fixed part of $\sim$ 6 $\mu C/cm^2$, which is comparable to the P_r of Hf-rich systems (~7 $\mu C/cm^2$). Thus, the difference part should result from defect dipoles, which align along the external field during the first run and stabilize. This difference also exists in the Zr-rich systems but is slightly lower in the numerical count ($\sim$ 7 $\mu C/cm^2$). Also, shifting the PE curve towards the left with increasing Zr-content indicates anti-site disordering in the systems. For TiN/HZO/TiN films grown by ALD and annealed at 600ºC showed anti-ferroelectric behavior and, when heated above 800ºC becomes resistive due to high leakage current along grain boundaries [30]. Minimura et al [31] deposited $HfYO_7$ film in the absence of oxygen through a sputtering process, and stabilized metastable O-phase was achieved attributed to oxygen vacancies. It is well-known that defect dipoles in the ferroelectric lattice led to high polarizability compared to the inherent ferroelectric polarization. In the present study,

8

metastable O-phase was observed at 500⁰C in a deposited thin film and is consistent with previous findings [19, 32]. The results of the PE analysis are shown in Table 2.

Table 2: Results of the PE analysis of HZO thin films.

Thin-films	E_r (MV/cm)	P_r (µC/cm^2)	P_{max} (C/cm^2)
Hf-rich	0.25	6.61	13.5
50-50	0.37	12.32	17.15
Zr-rich	0.39	10.52	14.89
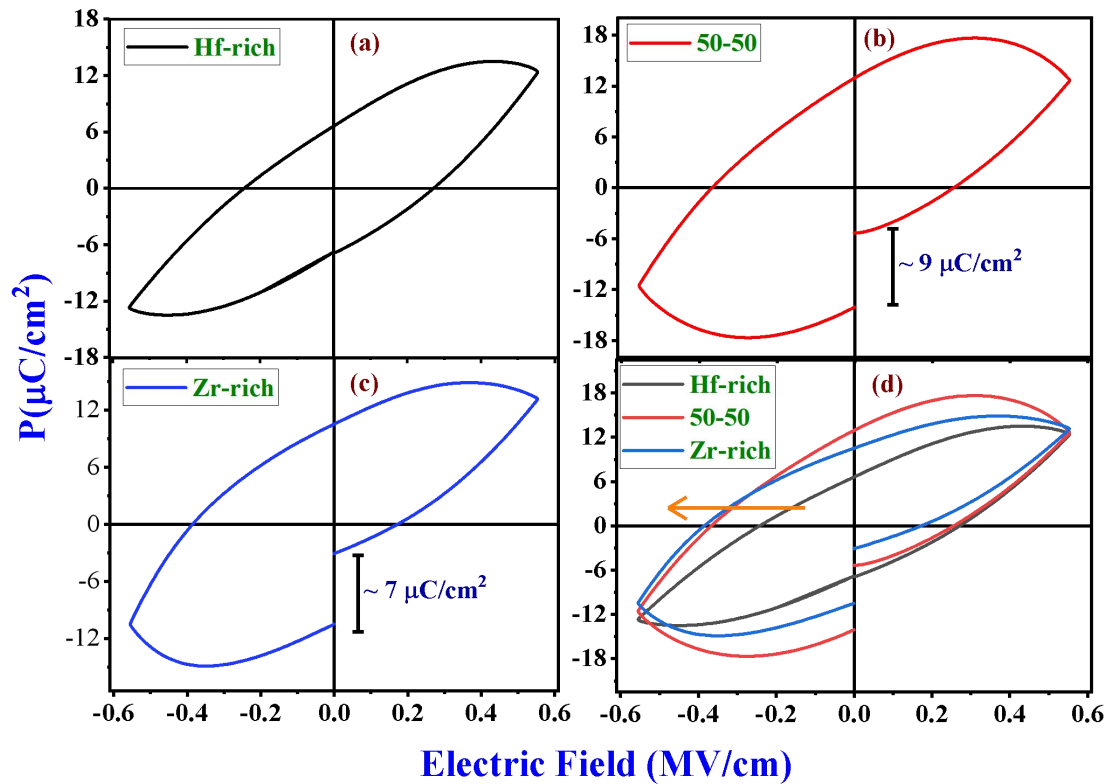
Figure-5 Polarization-Electric filed Hysteresis loop(a) Hf-rich (b) 50-50 (c) Zr-rich and (d) Comparative plot of HZO films

Dielectric analysis

Fig. 6 shows the (a) dielectric dispersion and (b) dielectric loss spectra of HZO films recorded at room temperature. The dispersion count of Hf-rich film is higher than others, indicating its' higher semi-insulating characteristics. The dispersion count decreases with increasing Zr content, which suggests that tuning the Zr-content, semi-metal characteristics of the HfO-

films can be tuned. The plateau feature of dispersion spectra indicates that the polarizability of available dipoles is forceless to follow the applied field frequencies.

On the contrary, in the tangent loss spectra of HZO films (see Fig. 6 (b)), the highest loss count value was observed for the Zr-rich system in the lower frequency regime. It could be the effect of electroplating, which dominates in the low-frequency regime. As the applied field frequency increases above 15 kHz, the loss count value of 50-50 film dominates. Here, the individual grain effect dominates over the grain boundary. However, the overall dielectric behavior of these films is consistent with their current density behavior. Such a lossy character of current density and dielectric behavior of the studied samples confirms the presence of defect-originated dipoles, as observed in XRD and XPS analysis.
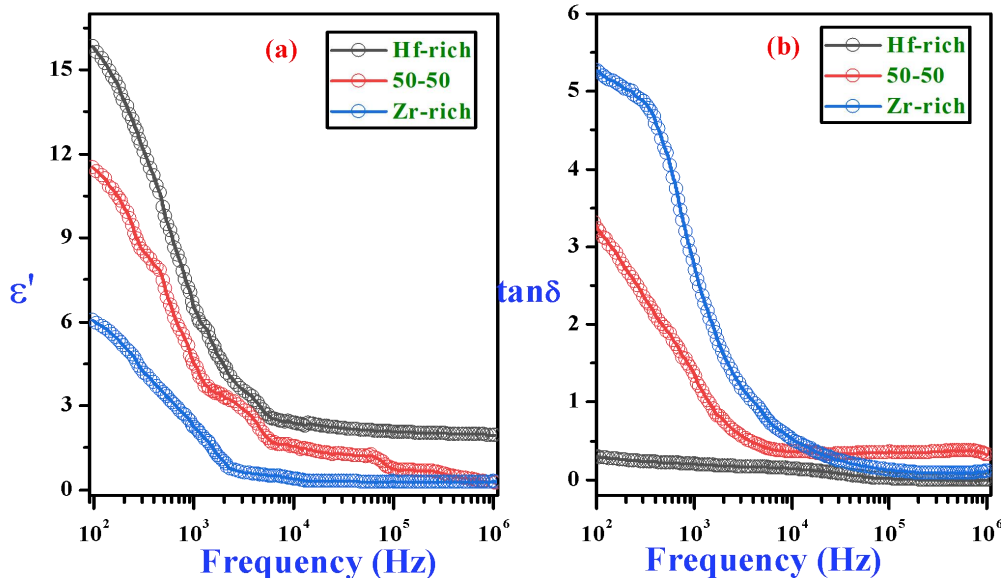
Figure 6: Frequency-dependent dielectric behavior of HZO films (a) dispersion and (b) loss spectra.

Conclusion

Studying the role of defect dipoles in the semiconducting ferroelectric thin films is a promising approach in understanding their anomalous behavior of electrical and ferroelectric response. Zr-modified, Hf-based thin films are successfully deposited using the CVBD technique. XRD and Raman spectra analysis showed a gesture of the defects due to cationic substitution. Although Hf and Zr have comparable ionic characters, it is not a common phenomenon to have sterically distorted crystal symmetry for these oxides. It could be possible due to a complex valance state in the cationic polyhedral. A detailed analysis of XPS spectra of 50-50 film confirmed the implicitness of the metallic and oxide bands of Hf-atoms

exclusively. These defect dipoles possessed the films current density, dielectric response, and ferroelectric behaviors of the films. The lossy and asymmetric PE loops are evidence of such defect-driven Ferro-character of HZO thin films. These defect dipoles carved a significant difference in the remnant polarization values during positive and negative cycles of the applied electric field. The observed difference results from defect dipoles aligning along the external field during the first run and stabilizing. Also, the shifting of the PE curve indicates anti-site disordering in the systems. Thus, we conclude that these HZO systems showed PE loops, lossy dielectric behavior, and high leakage current due to cationic defects.

References

[1] G D Wilk, J Appl. Phys. 89, 5243 (2001)

[2] G D Wilk, R M Wallace, J M Anthony, J Appl. Phys. 87, 484 (2000)

[3] J A Eastman, Nature 21, 838 (2022)

[4] T S Boscke, J Muller, D Brauhaus, U Schroder and U Bottger, Appl. Phys. Lett 99, 102903 (2011)

[5] N V Nguyen, Albert, V Davyadov, D Chandler-Horowitz; Appl. Phys. Lett. 87, 192903 (2005)

[6] K D Kim, M H Park, H J Kim, Y J Kim, T Moon, Y H Lee, S D Hyun, T Gwon, and C S Wang, J Mat Chem C, 4, 6864 (2016)

[7] K D Kim, M H Park, H J Kim, Y J Kim, T Moon, Y H Lee, S D Hyun, T Gwon, and C S Wang, J Mat Chem C, 4, 6864 (2016)

[8] X. Sang, E. D. Grimley, T. Schenk, U. Schroeder, James M. LeBeau, Appl. Phys. Lett. 106, 162905 (2015)

[9] S Mueller, J Mueller, A Singh, S Riedel, J Sundqvist, W Schroeder and Thomas Milkolajick, Adv. Funct. Mat. 22, 2412 (2012)

[10] A Chernikova,D S Kuzmichev, D V Negrov, M G Kozodeav, S N Polyakov and A M Markeev, Appl. Phys. Lett. 108 242905 (2016)

[11] J Müller, T S. Böscke, U Schröder, S Mueller, D Bräuhaus, U Böttger, L Frey, and T Mikolajick, Nano Lett. 12, 4318 (2012)

[12] M. Hoffmann, U. Schroeder, T. Schenk, T. Shimizu, H. Funakubo, O. Sakata, D. Pohl, M. Drescher, C. Adelmann, R. Materlik, A. Kersch, and T. Mikolajick, J Appl. Phys. 118, 072006 (2015)

[13] T Schenk, S Mueller, U Schroder, R Materlik, A Kresch, M Popovici, C Adelmann, S V Elshocht, T Mikalojick, Proceedings of the European Solid-State Device Research Conference (ESSDERC), Bucharest, Romania, B6L-C Emerging memories II, 260, (2013)

[14] T Shimizu, K Katayama, T Kiguchi, A Akama, T J. Konno, O Sakata & H Funakubo, Sc. Reports. 6, 32931 (2016)

[15] M H Park, H J Kim, Y J Kim, T Moon, and C S Hwang, Appl. Phys. Lett. 104, 072901 (2014)

[16] M H Park, H J Kim, Y J Kim, W Lee, H K Kim, and C S Hwang, Appl. Phys. Lett. 102, 112914 (2013)

[17] Y Wei, S Matzen, T Maroutian, G Agnus, M Salverda, P Nukala, Q Chen, J Ye, P Lecoeur, and B Noheda, Phys. Rev. Appl. 12, 031001 (2019)

[18] T Shimizu, T Yokouchi, T Shiraishi, T Oikawa, P. S. Sankara Rama Krishnan and H Funakubo, Jpn. J. Appl. Phys. 53 09PA04 (2014)

[19] P Nukala, J A -Lleonart, Y Wei, L Yedra, B Dkhil, and B Noheda, ACS Appl. Elec. Mater.1, 2585 (2019)

[20] L B-Lours, M Mulder, P Nukala, S de Graaf, Y A. Birkhölzer, B Kooi, B Noheda, G Koster, and G Rijnders, Phys. Rev. Materials 4, 043401 (2020)

[21] J. Zhu, L. Chen, J. Jiang, X. Lu, L. Yang, B. Hou, M. Liao, Y. Zhou, X. Ma, and Y. Hao, IEEE Electron Device Lett. 39, 79 (2018)

[22] R Rani, W Maudez, R Sayal, R Rai, S Kumar, Md K Shamim, E Wagner, S Sharma and G Benvenuti, Phys. B: Cond. Mat. 650, 414541 (2023)

[23] R Rani, Md K Shamim, W Maudez, , E Wagner, R Rai, S Sharma and G Benvenuti, Thin Solid Films. 778, 139883 (2023)

[24] S Starschich, D Griesche, T Schneller, U Bottger, ECS J Sol. St. Tech. 3, P419 (2015)

[25] M Pesic, M Hoffman, C Richter, T Mikolajick, U Schroeder, Adv Func Mater. 26, 7489 (2016)

[26] J Lyu, I Fina, J Fontcuberta, F Sanchez ACS Appl. Mater. Interfaces 11, 6224 (2019)

[27] C Zacharaki, P Tsipas, S Chaitoglou, S Fragkos, M Axiotis, A Lagoyiannis, RNegrea, L Pintilie, A Dimoulas, Appl. Phys. Lett. 114, 112901 (2019)

[28] B Zhou,H Shi,X D Zhang, Q Su, and ZY Jiang, J Phys. D Appl. Phys. 47, 115502 (2014)

[29] X Zhao, and D Vanderbilt, Phys Rev B 65, 233106 (2002)

[30] M N Lee, Y.-T. Wei, C. Liu, J.-J. Huang, M Tang, Y-L Chueh, K.-Y. Chu, M-J Chen, H-Y Lee, Y-S Chen, L-H Lee, and M-J Tsai, J Eel. Dev. 3, 377 (2015)

[31] T Minmura, T Shimizu, H Uchida, H Funakubo, Appl. Phys. Lett. 116, 062901 (2020)

[32] T Kiguchi, S Nakamura, A A Kama, T Shiraishi and T J. Konno; J Ceram. Soc. Japan 124, 689 (2016)